INTERNATIONAL JOURNAL OF INNOVATIVE RESEARCH & DEVELOPMENT

ISSN 2278 – 0211 (Online)

Hydrodynamic and Electro-Osmotic Studies on Transport through Nylon-66 Membrane Using Aqueous Aluminium Nitrate as Permeant

Manoj Kumar
Ph.D. Scholar, Department of Chemistry, Centre of Advanced Study,
Faculty of Science, Banaras Hindu University, Varanasi, U.P., India
Bali Ram
Professor, Department of Chemistry, Centre of Advanced Study,
Faculty of Science, Banaras Hindu University, Varanasi, U.P., India

Abstract:
The object of this work was to study the transport phenomena across the nylon-66 membrane of aqueous aluminum nitrate as permeants. Hydrodynamic and electro-osmotic permeability measurements of water and aqueous solutions of Al $(NO_3)_3.9H_2O$ in the concentration range of 10^{-4} M to 10^{-3} M have been made. The data obtained have been used to determine the transport equation using the theory of non-equilibrium thermodynamics. Streaming current generated during the transport of various permeants was also measured and its dependence on pressure investigated. Phenomenological coefficients have been determined using the transport equation and Saxen's relationship verified. Zeta potentials have been evaluated using electro-osmotic permeability and membrane-permeant conductance data. It has been observed that hydrodynamic and electro-osmotic permeabilities depend linearly on applied pressure difference and potential difference respectively.

Keywords: *Non-equilibrium thermodynamics, Nylon-66 membrane, Electro-osmotic flux, Streaming potential and Zeta potential*

1. Introduction

There are so many industrial applications of nylon membranes, which are most commonly used polymer for fabrication of gears, bearings, fibers, etc. [1]. Nylon was the first synthetic polyamide with super thermal stability and mechanical strength, allowing it to be classified as an engineering thermoplastic. The polymer of Nylon (polycaprolactam) is widely used as a membrane material for the application in biotechnology and medicine as drug delivery systems. Porosity of the nylon membrane was found to increase with increasing water substance in the dope. This was evidenced by the tensile strength and water permeability measurements [2]. Unlike other commercial membranes, this membrane carries a microporous character being composed of micron-sized crystallites that interlock into a uniform bi-continuous structure and particularly, it is inherently wetted by water due to the microcapillarity within the membrane structure. As a result, membrane is employed extensively in aqueous micro-filtration applications [3-4].

According to the theory of non-equilibrium thermodynamics of steady states [5-7] fluxes are coupled, which can be identified using thermodynamic principles. These fluxes obey linear phenomenological relations and a stable steady state. Non-equilibrium steady states can also be stable even when the phenomenological relations are nonlinear [8-10].

In the present article, we have used a nylon-66 membrane to study the transport of aqueous Al $(NO_3)_3.9H_2O$ and the results have been analyzed on the basis of the theory of non-equilibrium thermodynamics of irreversible processes. Streaming current generated during the transport of various permeants was also measured for verifying Saxen's relationship. The results obtained with these studies may be helpful in understanding the electrical nature of the membrane-permeant interface [11].

2. Experimental

2.1. Materials

Nylon-66 membrane (Cat No -170025P) used in this study was procured from Axiva Sichem Biotech, New Delhi and it was fitted in the experimental cell for study. Al $(NO_3)_3.9H_2O$ (SDFCL, Hyderabad) was used as such without further purification to

prepare aqueous solutions using doubly distilled water. Aqueous solutions of this salt in the concentration range of 10^{-4} M to 10^{-3} M were used as permeants during measurements.

2.2. Scanning Electron Microscopy (SEM) Analysis

The microstructure of the membrane was studied using scanning electron microscope (Model - QUANTA 200 F) before fixing it in the experimental cell. Images of nylon-66 membrane were taken at different magnification range as shown in Figure 1 (a & b), in order to see the surface morphology and pore size distribution.

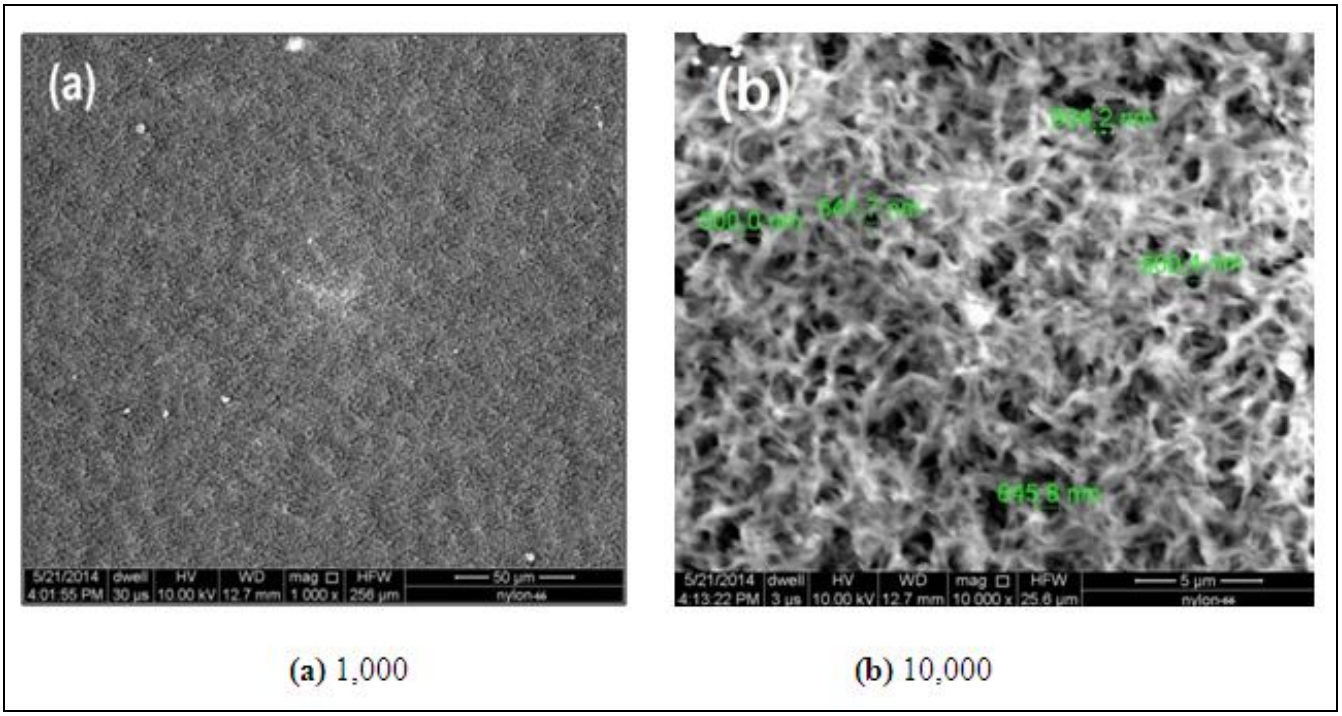

Figure 1: SEM images of the top surface area at different magnification

2.3. Measurement of Hydrodynamic Permeability

Hydrodynamic permeability was measured by using an experimental setup, already described by many workers [11-12]. The experimental cell was filled with the liquid under investigation, and left as such for 10 to 12 hours for equilibration before use. For maintaining the equilibrium, the cell was subsequently filled with a degassed fresh solution to confirm that the concentration of the experimental solution remained the same on both sides of the membrane. The volume flux across the membrane under various pressure differences was measured by monitoring the movement of liquid-air meniscus in a horizontally placed graduated capillary tube with a cross sectional area of 7.86×10^{-7} m^2. The values of transport coefficients (L_{11}/T) determined from the data on permeability measurement are recorded in the Table 1.

2.4. Measurement of Electro-Osmotic Permeability

Electro-osmotic permeability was measured by the same experimental cell as described above. Pt-electrodes were fitted in the experimental cell in such a way as to touch the membrane from both the sides. Potential differences in the range of 10 to 50 V were applied across the membrane through electrodes with the help of an electronically operated power supply (Medox-Bio, Power Supply 300 Advanced). The volumetric flux was measured by following the rate of displacement of the liquid-air meniscus in a horizontally placed graduated capillary tube with a cross sectional area of 7.86×10^{-7} m^2. The values of electro-osmotic transport coefficients (L_{12}/T) determined from the permeability measurement data are recorded in the Table 1. All experiments were carried out in air thermostat maintained at 30 ± 0.5^{o} C.

2.5. Measurement of Streaming Current

Streaming current generated during the transport of permeants by application of various pressure differences on the two sides of the membrane were measured with a Digital Picoammeter (Model PM-100, Raman Scientific Instruments, Roorkee, India) by the technique described elsewhere [12]**.** The streaming current at lower pressure could not be measured correctly due to less sensitivity of the instrument. The values of transport coefficients (L_{21}/T) determined from the streaming current measurement data are recorded in the Table 1.

2.6. Measurement of Membrane Conductance

The conductivity of the membrane equilibrated with permeants (L_{22}/T) and specific conductance (χ) of permeants were measured with the help of conductivity meter (Systronics-304, cell constant 1± 0.1). The values of membrane conductance (L_{22}/T) and specific conductance (χ) were found to be in increasing order due to increasing concentrations of the solution and are recorded in the Table 1 and 2 respectively.

C × 10^4 (M)	$\frac{L_{11}}{T}\times10^{13}$ **($m^5 s^{-1} N^{-1}$)**	$\frac{L_{12}}{T}\times10^{10}$ **($m^3 s^{-1} v^{-1}$)**	$\frac{L_{12}}{T}\times10^{10}$ **($m^3 s^{-1} v^{-1}$)**	$\frac{L_{22}}{T}\times10^{5}$ **(Sm^{-1})**
0.0	10.69	1.78	1.78	3.60
1.0	10.04	1.67	1.66	5.40
2.0	9.35	1.54	1.51	10.20
4.0	8.47	1.43	1.46	18.60
6.0	8.26	1.27	1.25	27.00
8.0	7.98	1.16	1.15	35.00
10.0	7.53	1.05	1.07	44.00

Table: 1 Phenomenological coefficients for Al $(NO_3)_3.9H_2O$-aqueous system

C × 10^4 (M)	**η × 10^3 (poise)**	**ϰ × 10^5 (Sm^{-1})**	**r × 10^7 (m)**	**n × 10^{-7}**	**Km × 10^3 (m)**	**$\zeta_{e.o.}$ × 10^3 (V)**
0.0	6.08	5.07	8.557	0.926	7.101	21.566
1.0	6.10	5.63	7.147	1.794	9.591	15.007
2.0	6.23	10.40	6.893	1.953	9.807	13.822
4.0	6.37	18.59	6.568	2.216	10.005	12.864
6.0	6.51	25.00	6.311	2.591	10.800	10.451
8.0	6.67	31.70	6.210	2.735	11.041	9.902
10.0	6.80	39.10	6.033	2.954	11.253	8.965

Table: 2 Membrane parameters for Al $(NO_3)_3.9H_2O$-aqueous system

2.7. Measurement of Viscosity of Permeants

The values of viscosity are recorded and are shown in the Table 2. Ostwald viscometer was used for determining the viscosity (η) of each solution.

$$\eta_1 = \eta_2 \times \frac{t_1 d_1}{t_2 d_2}$$

Where, η_1 is viscosity of aqueous solutions and η_2 is viscosity of conductivity water.
t_1 is time of flow of aqueous solutions and t_2 is time of flow of conductivity water.
d_1 is density of aqueous solutions and d_2 is the density of conductivity water.

3. Results and Discussion

Non-equilibrium thermodynamic theory [13] shows that volume flux, J_v, and electrical current, I, under the simultaneous action of pressure difference (ΔP) and electrical potential difference ($\Delta\phi$) are given by:

$$J_v = \frac{L_{11}}{T}(\Delta P) + \frac{L_{12}}{T}(\Delta\phi) \quad (1)$$

$$I = \frac{L_{21}}{T}(\Delta P) + \frac{L_{22}}{T}(\Delta\phi) \quad (2)$$

Where, I is the flow of electricity and the quantities L_{mn} (m, n = 1, 2) are called the phenomenological coefficients.
When, $\Delta\phi = 0$, Eq. (1) reduces to

$$(J_v)_{\Delta\phi=0} = \frac{L_{11}}{T}(\Delta P) \quad (3)$$

Hydrodynamic volume flux, J_v, was found to show a linear dependence on the applied pressure difference, ΔP. The plots of $(J_v)_{\Delta\phi = 0}$ against ΔP as shown in Figure 2 are straight lines.
When, $\Delta P = 0$, Eq. (1) reduces to

$$(J_v)_{\Delta P=0} = \frac{L_{12}}{T}(\Delta\phi) \quad (4)$$

The electro-osmotic volume flux $(J_v)_{\Delta P = 0}$ against $\Delta\phi$ plots are also found linear and shown in Figure 3.

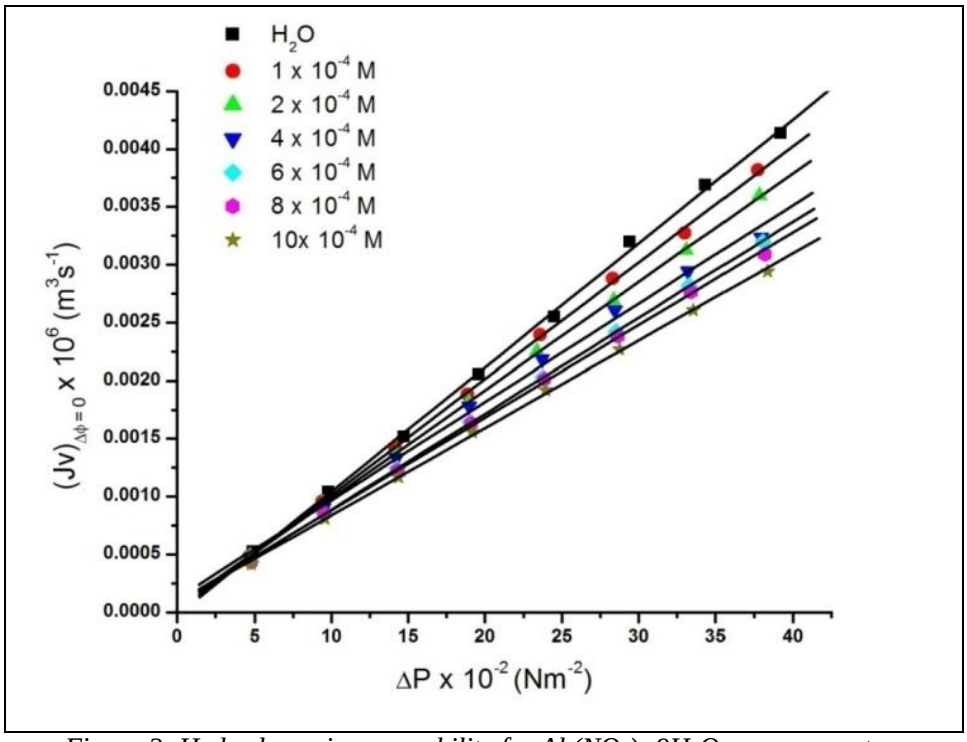

Figure 2: Hydrodynamic permeability for Al $(NO_3)_3.9H_2O$-aqueous system

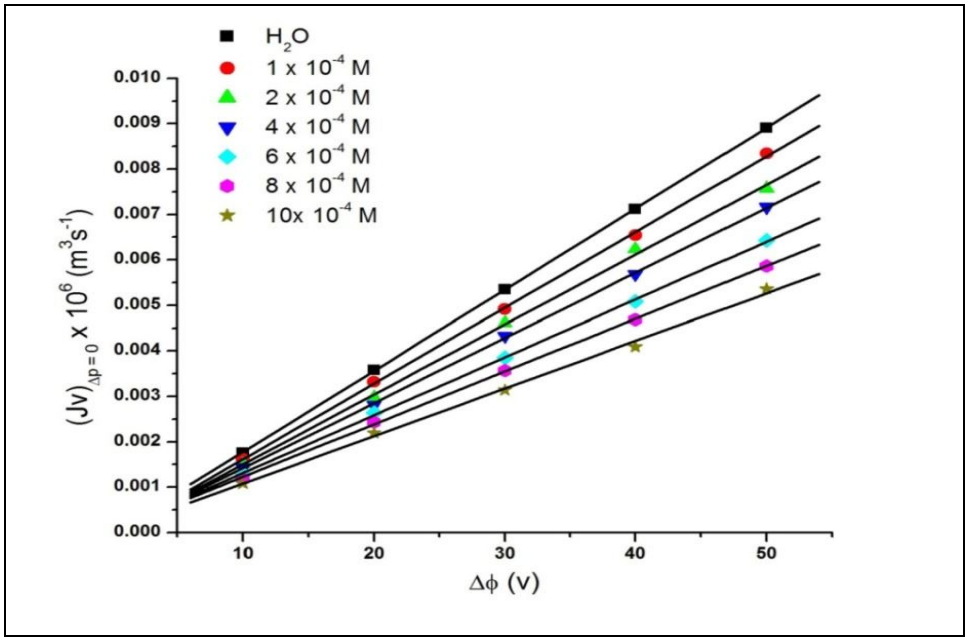

Figure 3: Electro-osmotic flux for Al $(NO_3)_3.9H_2O$-aqueous system

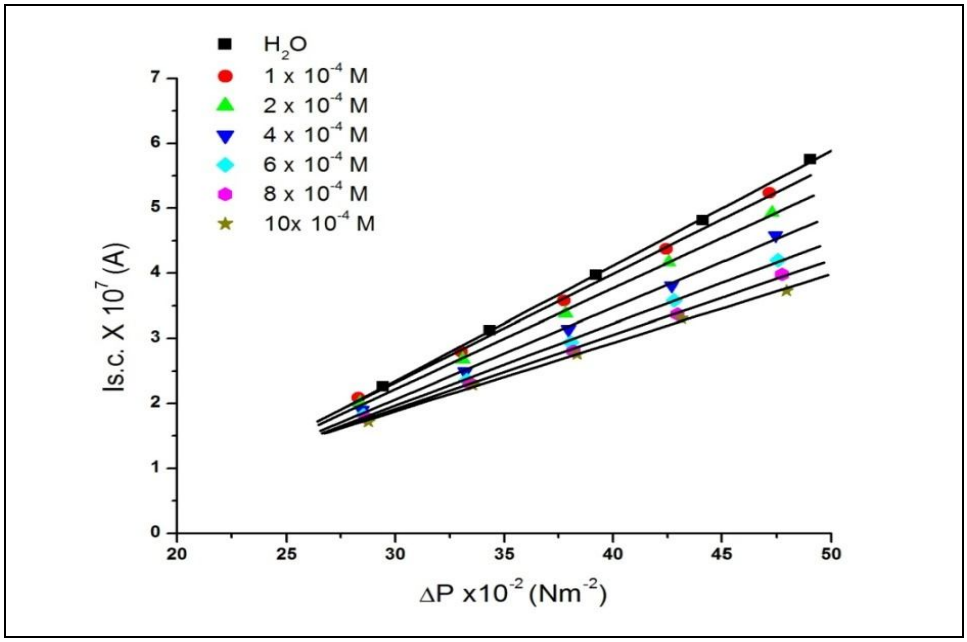

Figure 4: Streaming current for Al $(NO_3)_3.9H_2O$-aqueous system

The values of phenomenological coefficients (L_{11}/ T) and (L_{12}/T), obtained from the slopes of linear plots of $(J_v)_{\Delta\phi=0}$ vs. ΔP and $(J_v)_{\Delta P=0}$ vs. Δϕ respectively, are recorded in the Table 1.
When, Δϕ = 0; Eq. (2) gives

$$(I)_{\Delta\phi=0} = \frac{L_{21}}{T}(\Delta P) \tag{5}$$

Where $(I)_{\Delta\phi=0}$ is streaming current.
The plots of $(I)_{\Delta\phi=0}$ against ΔP as shown in Figure 4 are straight lines, with slopes of giving the values of phenomenological coefficient (L_{21}/T), are recorded in the Table 1.
Following the theory of Overbeek [14] for the flow of liquid through single capillary; we have,

$$\frac{L_{21}}{T} = \frac{\pi r^4}{8\eta\ell} \tag{6}$$

$$\frac{L_{12}}{T} = \frac{\epsilon r^2 \zeta}{4\eta \ell} \quad (7)$$

$$\frac{L_{22}}{T} = \frac{\pi r^2 \chi}{\ell} \quad (8)$$

If the flow occurs through a membrane which consists of parallel arrays of *n* capillaries, the right hand side of above equation would increase *n* times. Therefore,

$$\frac{L_{11}}{T} = \frac{n\pi r^4}{8\eta \ell} \quad (9)$$

$$\frac{L_{12}}{T} = \frac{n\epsilon r^2 \zeta}{4\eta \ell} \quad (10)$$

$$\frac{L_{22}}{T} = \frac{n\pi r^2 \chi}{\ell} \quad (11)$$

An observation of the Table 1 shows that the values of L_{11}/T decreases with increase in the concentration of permeants which may be attributed to increase in viscosity of permeants. The values of electro-osmotic permeability coefficients (L_{12}/T) are also found in decreasing order which may be due decrease in the value of zeta potential caused by the appearance of an increasing amount of ions due to electrolysis. The values of L_{22}/T i.e. conductance of membrane- equilibrated with permeants, was found in increasing order with increase in the concentration of the permeants. These results are commensurate with the conductance values of the respective solutions. Measurement of conductance of membrane-equilibrated with permeants is useful to get insight into the electro-kinetic properties of the membrane porous bodies [15] which depend on the pore size and the zeta potential of the membrane. The electrical conductivity inside the membrane may be higher than the bulk conductivity [16], these effects happen due to high salt concentrations.

Electro-osmotic flux occurs towards the anode i.e. from negative to positive electrode. This may be explained on the basis of electrical double-layer supposed to be formed at the membrane-permeant interface, as shown in Figure 5. The nylon-66 membrane has the following molecular structure.

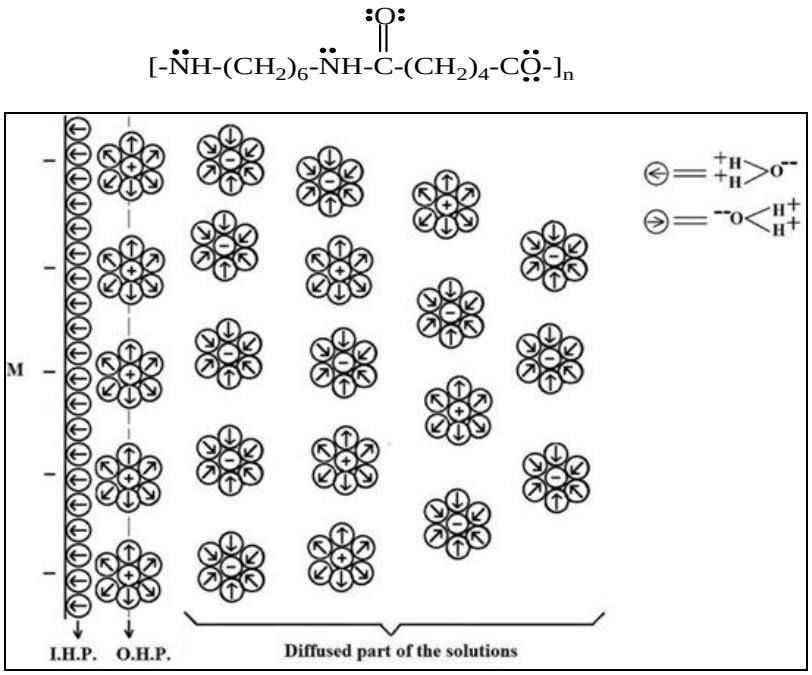

Figure: 5 Postulated Picture of the electrical double layer at the nylon-66/aqueous solution interface

I.H.P. = Inner Helmholtz Plane
O.H.P. = Outer Helmholtz Plane
M = Membrane Surface
⊕ = Cations
⊖ = Anions

The presence of the lone pair of electrons on nitrogen and oxygen atoms in the molecular structure of nylon-66 might be collectively responsible for generating an overall negative charge on the membrane surface. The hydrated cations are adsorbed on the surface of membrane matrix, leaving behind excess of hydrated anions, which moves towards the positive electrode on the application of electrical potential across the membrane.
Examination of Table also reveals that the values of L_{12}/T (obtained from electro-osmotic transport equation) and L_{21}/T (obtained from streaming current measurement) are nearly equal, i.e. $L_{12}/T \approx L_{21}/T$; thereby indicating the validity of Saxen's relationship.

3.1. Characterization of the Membrane
Most of the transport properties of membranes depend on the characteristics of the membrane itself. The characterization of nylon-66 membrane was achieved by scanning electron microscope technique (SEM) analysis as well as Pore radii (r), average number of pores (n) and membrane constant (K_m) were evaluated using the formula given by Srivastava and Ram [11-12].

3.1.1. Morphological studies of Nylon-66 membrane
The Scanning Electron Microscope (SEM) technique was used to characterize the top surface-morphological structure of the nylon-66 membrane. Membrane was snapped in different magnification range (Model - QUANTA 200 F). It was observed that at low magnification the membrane shows very small pore, muddy like structure and at high magnification it shows macro pores having different pore sizes which are shown in the image. The SEM images are shown in the Figure 1. In general, it is thought that morphology of the membrane having muddy like structure contributes to give a better response for solute permeation.

3.1.2. Determination of pore radii, average number of pores and membrane constant
From equation (9) and (11), pore radii (r) follow that

$$r^2 = \frac{8\eta\chi\,(L_{11}/T)}{(L_{22}/T)}$$

or

$$r = \sqrt{\frac{8\eta\chi\,(L_{11}/T)}{(L_{22}/T)}} \qquad (12)$$

where χ and η are the conductance and viscosity of the permeants, respectively.
From equation (11), average number of pores (n) follows that

$$n = \frac{(L_{22}/T)\ell}{\pi r^2 \chi} \qquad (13)$$

Where L_{22}/T is the conductance of membrane-permeant system and ℓ is the thickness of the membrane.
From equation (11), we have

$$\frac{L_{22}}{T} = \frac{n\pi r^2 \chi}{\ell} \quad \text{or} \quad \frac{L_{22}}{T} = \frac{A_e}{\ell}\chi\,,$$

Where $A_e = n\pi r^2$ is the effective cross sectional area of the membrane through which permeation occurs. Hence, membrane constant K_m is given as

$$K_m = \frac{A_e}{\ell} = \frac{L_{22}/T}{\chi} \qquad (14)$$

The values of these membrane parameters are shown in the Table 2.
The values of pore radii are found in decreasing order with increasing concentration which indicates that on increasing concentration the pores of membrane become narrow size. It may also depend on the values of phenomenological coefficients. The permeating particles are much smaller than the pore size of the membrane and therefore enter into the membrane pores and adhere to the internal pore walls. Due to this reason, the membrane pore volume decreases proportionally with the permeate volume with increasing concentration. It is assumed that the permeating particles arriving to the membrane surface can restrict the flow to some extent.

3.2. Determination of Zeta Potential

Generally the zeta potentials of the membranes are supposed to represent the chemical nature of the membrane materials, which is fundamental feature and provides useful information about the electrical charge at solid-liquid surface. Evaluation of zeta potential of membranes is particularly attractive because this quantity is correlated with the mechanism of rejection of charged solutes [17]. In various solutions, electrical nature of the membrane-interfaces can be expressed in terms of zeta potential, which is estimated by combining the electro-osmotic flux coefficient (L_{12}/T) with the membrane-permeants conductance (L_{22}/T).

Zeta potentials from electro-osmotic measurements ($\zeta_{e.o.}$) were estimated from the following equation [11, 18-19].

$$\zeta_{e.o.} = \frac{4\pi\eta\chi\,(L_{12}/T)}{\epsilon(L_{22}/T)} \times 9 \times 10^{7}\ \text{mV} \qquad (15)$$

Where, ϵ is the dielectric constant of the medium used, i.e. water. The values of zeta potentials estimated in this way are recorded in the Table 2. The data for zeta potential obtained from the study on membrane indicate that it decreases with increasing concentration of solutions. The differences in the behavior of zeta potential can be explained on the basis of an altered structure of water [20] which is likely to affect the electro-osmotic behavior marginally.

4. Conclusion

Sorption takes place in the membrane matrix due to accumulation of electrolyte ions in membranes. Thermodynamic theory of irreversible processes confirms the validity of the linear phenomenological relations, and zeta potential values indicate the existence of electrical charge on membrane surface which also gives information about the net charge on the surface as well as the charge distribution inside the electric double layer (EDL). The SEM analysis also confirms that CA membrane having different sizes of small pores and fine surface morphology may be useful for numerous purposes in separation areas also. Sometimes evolution of gases occurs at the electrodes due to polarization which may occur when higher electrical potentials are applied across the electrodes; this was, however, minimized by using freshly boiled conductivity water for filling the apparatus.

5. Acknowledgments

Authors would like to thank Banaras Hindu University, Varanasi, for the laboratory facilities and University Grant Commission, New Delhi, for financial support as the Rajiv Gandhi National Fellowship. We also thank, the Department of Metallurgical Engineering IIT-BHU, Varanasi for SEM analysis of the membrane.

5.1. List of Symbols

- A_e Effective cross-sectional area of membrane (m^2)
- I Electric current (A)
- J_v Volume flux (m^3s^{-1})
- K_m Membrane constant (m)
- L_{11} Phenomenological coefficient representing hydrodynamic permeability ($m^5\,s^{-1}N^{-1}$)
- L_{12} Phenomenological coefficient representing electro-osmotic permeability ($m^3\,s^{-1}V^{-1}$)
- L_{21} Phenomenological coefficient representing streaming potential ($m^3s^{-1}V^{-1}$)
- L_{22} Phenomenological coefficient representing conductivity he membrane-permeant system of (Sm^{-1})
- ℓ Length of pore channel (m)
- n Average number of pores
- ΔP Pressure difference (Nm^{-2})
- r Equivalent pore radii (m)
- C Concentration (M)

5.2. Greek Symbols

- ϵ Dielectric constant of the medium
- $\zeta_{e.o.}$ Zeta potential calculated from electro-osmotic flux data (V)
- η Viscosity coefficient (Poise)
- χ Specific conductance (Sm^{-1})
- $\Delta\phi$ Electrical Potential difference (V)

6. References

1. M. I. Kohan, Nylon Plastics Handbook, Hanser/Gardner, New York, 1995.
2. L. P. Cheng, D. J. Lin, and K. C. Yang, Formation of mica-intercalated-Nylon 6 nanocomposite membranes by phase inversion method, J. Membr. Sci., 172 (2000), 157–166.
3. U. V. Stockar, The role of thermodynamics in biochemical engineering, J. Non-Equilib. Thermodyn., 38 (2013), 225–240.
4. U. V. Stockar, Optimal energy dissipation in growing microorganisms and rectification columns, J. Non-Equilib. Thermodyn., 39 (2014), 3-11.
5. I. Prigogine, Introduction to thermodynamics of irreversible processes, 2nd revised edn. Interscience, New York, 1961.
6. K. G. Denbigh, Thermodynamics of steady state, Wiley, New York, 1951.
7. S. R. de Groot, Thermodynamics of irreversible processes, North-Holland, Amsterdam, 1952.
8. R. P. Rastogi, R. C. Srivastava, P. Chand, Membrane oscillations involving electrokinetic phenomena, J. Colloid Interface Sci. 263 (2003) 223-227.
9. R. P. Rastogi, R. C. Srivastava, S. N. Singh, Nonequilibrium thermodynamics of electrokinetic phenomena, Chem. Rev. 93 (1993) 1945-1990.
10. R. P. Rastogi, R. C. Srivastava, Interface-mediated oscillatory phenomena, Adv. Colloid Interface Sci. 93 (2001) 1-75.
11. M. L. Srivastava, B. Ram, Electrokinetic studies of the testosterone- aqueous d-glucose interface, Carbohydr. Res. 132 (1984) 209-220.
12. M. L. Srivastava, B. Ram, Electrokinetic studies on testosterone/aqueous electrolyte interface: Part 1. Electro-osmosis, electrophoresis, streaming potential and streaming current. J. Membrane Sci. 19 (1984) 137-153.
13. A. Katchalsky, P. F. Curran, Non-equilibrium Thermodynamics in Biophysics, Harvard University Press, Cambridge, MA, 1965.
14. J. T. G. Overbeek, H. R.Kruyt, Ed., Colloid Science 1, Elsevier, Amsterdam & New York, 1952.
15. A. E. Yaroshchuk, T. Luxbacher, Interpretation of electrokinetic measurements with porous films: role of electric conductance and streaming current within porous structure, Langmuir 26 (2010) 10882-10889.
16. A. Szymczyk, P. Fievet, B. Aoubiza, C. Simon, J. Pagetti, An application of the space charge model to the electrolyte conductivity inside a charged microporous membrane, J. Membrane Sci. 161 (1999) 275-285.
17. C. Labbez, P. Fievet, F. Thomas, A. Szymczyk, A. Vidonne, A. Foissy, P. Pagetti, Evaluation of the "DSPM" model on a titania membrane: measurements of charged and uncharged solute retention, electrokinetic charge, pore size, and water permeability, J. Colloid Interface Sci. 262 (2003) 200-211.
18. R. Shabd, B.M. Upadhyay, Electrokinetic studies on carbohydrates, Carbohydr, Res. 90 (1981) 187-192.
19. R. Shabd, B.M. Upadhyay, Electrokinetic studies on cholesterol-carbohydrate systems, Carbohydr. Res. 93 (1981) 191-196.
20. R. E. Kesting, Synthetic Polymeric Membranes, McGraw-Hill, New York, 1971.